NI

NASA Technical Memorandum 81316

USAAVRADCOM TR-81-A-25

The Structure of Trailing Vortices Generated by Model Rotor Blades

C. Tung, S. L. Pucci, F. X. Caradonna
and H. A. Morse

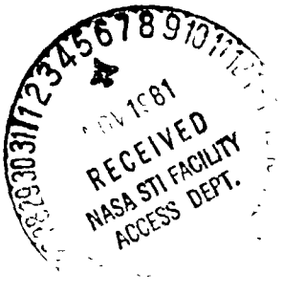

August 1981

National Aeronautics and Space Administration

United States Army Aviation Research and Development Command

NASA Technical Memorandum 81316

USAAVRADCOM TR-81-A-25

The Structure of Trailing Vortices Generated by Model Rotor Blades

C. Tung,
S. L. Pucci,
F. X. Caradonna,
H. A. Morse, Aeromechanics Laboratory
AVRADCOM Research and Technology Laboratories
Ames Research Center, Moffett Field, California

National Aeronautics and Space Administration

Ames Research Center
Moffett Field, California 94035

United States Army
Aviation Research and Development Command
St. Louis, Missouri 63166

ABSTRACT *

The present study is one of a series of tests employing hot-wire anemometry to investigate the effects of blade geometry on vortex structure. These tests cover a range of aspect ratios and blade twist. For all configurations, measured vortex strength correlates well with maximum blade-bound circulation. Measurements of wake geometry are in agreement with classical data for high aspect ratios. The detailed vortex structure is similar to that found for fixed wings and consists of four well-defined regions — a viscous core, a turbulent mixing region, a merging region, and an inviscid outer region. All high aspect ratio data are described by a single set of empirical formulas.

LIST OF SYMBOLS

A = ratio of vortex circulation to maximum blade-bound circulation

A_V = input constant value of A

C_Q = torque coefficient

C_T = thrust coefficient

d = distance from the center of a vortex

FM = figure of merit

R = radius of the rotor blade

r = radial distance from the rotor center of rotation

r_1 = radius of a vortex where the tangential velocity reaches maximum value

V_i = vortex-induced velocity

V_R = residual velocity in the wake

V_T = tip velocity

V_{TR} = vortex translation velocity

Z = axial distance from rotor

Ω = rotational speed

Γ = circulation

---

*Paper was presented at the Seventh European Rotorcraft and Powered Lift Aircraft Forum, September 8-11, 1981, Garmisch-Partenkirchen, Federal Republic of Germany.

Γ_{max} = maximum blade-bound circulation

ψ = azimuthal angle measured from the point of blade overhead passage

ψ_v = vortex age when vortex strikes the probe

θ_c = collective pitch angle

1. Introduction

The latest generation of hover prediction methods should be accurate to within 2% to be useful. This accuracy requirement places a severe strain, not only on computational methods, but also on the available body of rotor wake knowledge. As part of a reexamination of this rotor wake knowledge, the U.S. Army Aeromechanics Lab has begun a series of tests designed to simultaneously obtain blade wake and loading data. The initial phases of these tests were reported in Ref. [1]. In this test, detailed blade surface pressure distributions on a low aspect ratio blade were obtained simultaneously with hot-wire measurements of the locations and structure of the shed tip vortices. It was shown that blade loading could be well predicted using the measured wake characteristics as prescribed input. However, the measured geometry (especially the contraction) of the vortex differed from other published data (Ref. [2]) for low aspect ratio blades. Furthermore, the vortex strength, found using the Cook fitting technique, closely matched the maximum bound circulation. This latter result differed markedly from Cook's original results and was attributed to differences in the number of blades, twist, and aspect ratio.

In the present paper, we describe an experiment similar to that of Ref. [1], but performed on high aspect ratio twisted and untwisted blades. The purpose of this test is to check the possibility of anomalous results due to test chamber effects and to assess the possible effects of blade geometry on vortex strength. It will be shown that, unlike the low aspect ratio results, tests on the high aspect ratio blades produce vortex trajectories which are in good agreement with previously published data. Furthermore, all tests indicate that at typical operating conditions, the vortex strength equals the maximum blade-bound circulation. In addition, special attention is given to the inner viscous core region of the vortex. It will be shown that, with minor exceptions, the structure of this region is not a function of any of the tested blade geometry characteristics.

2. The Experiment

The experiment was performed in the Army Aeromechanics Lab Anechoic Hover Chamber (AHC) — a large cubic room (about 10 m on a side) with special ducting designed to eliminate room recirculation. As in Ref. [1], the rotor was situated in the center of the chamber, mounted on a tall column containing the drive assembly (Fig. 1). The wake data acquisition process is described in Ref. [1]. Briefly stated, the method was to use a traversing single hot-wire probe to find a number of points along the tip vortex trajectory. The probe was oriented parallel to the vortex axis to eliminate sensitivity to the axial components of velocity. From the time history of the hot-wire velocity measurement, the vortex strength and structure can be inferred. An often-mentioned problem with this technique is that the rotor wake is unsteady and the vortex trajectory region is, in reality, a fairly wide band rather than a single line. Finding the center of this band is a time-consuming task, and the data obtained at that point are still very unsteady. The best solution to this problem seems to be a careful screening (by digital techniques) of the acquired data such that the only data analyzed are those in

which the vortex core makes a direct hit on the hot wire. Such a hit and the above-mentioned unsteadiness are shown in Fig. 2.

A major difference between the present work and Ref. [1] is that rotor loads are obtained from a six-component balance rather than by an integration of the measured pressure distribution. It was found in Ref. [1] that the predicted blade-load distribution obtained by available lifting-surface codes [3] agreed well with surface pressure instrumentation. Therefore, measurements of the blade surface pressures were not considered to be essential for this test. The approach used to find the load distribution is to measure the wake geometry, which is used as prescribed input to a lifting surface code (in this case the A.M.I. code HOVER). If the measured and predicted thrusts compare well (as is almost always the case), it is assumed that the predicted lift distribution is also accurate.

The rotor blades tested were all untapered planform blades (NACA 0012 airfoil) with an aspect ratio of 13.7 and a radius of 104.5 cm. One set of blades is untwisted, while the other set has a linear twist of 8° from 0.2 radius to the tip. The goal of the test is to compare the strength and structure of the tip vortices for twisted and untwisted blades. In comparing the wake of the twisted and untwisted rotors, the thrust of the two rotors must be adjusted such that their maximum bound circulations are equal. These operating conditions are determined by means of an appropriate loads code.

3. Data Reduction and Analysis

The first step in finding the required operating conditions is the determination of the vortex trajectories. This step was considered necessary because of the lack of agreement between low aspect ratio results of Ref. [1] and previously published data [2]. In fact, all the high aspect ratio trajectory data are in excellent agreement with classical wake data (Fig. 3). We currently have no explanation for the low aspect ratio discrepancy. The consistency of the measured wake with predicted and measured loading does seem to rule out measurement error as a possibility. Certainly, the good agreement of the high aspect ratio results with classical data indicates a basic soundness of the hover test facility, and in subsequent computations of blade loading it was possible to use either Landgrebe's or Kocurek's prescribed wake data.

In using the loads program to determine operating conditions, it is necessary to specify the vortex strength. This seems premature, since the determination of vortex strength is a primary goal of the test. Nevertheless, the simplification of the traditional "fully rolled-up" assumption is compelling and, as will now be shown, works very well. Table 1 is a comparison of measured and predicted performance for the rotors with twisted and untwisted blades. Included in this table are results for three collective angles (5°, 8°, and 12°) for the untwisted blade rotor. Corresponding to these are two groups of results for the rotor with twisted blades – one set calculated to match the thrust of the rotor with untwisted blades, and one set to match the maximum bound circulation on the two rotors.

The comparison between measured and predicted thrusts is quite good, except at the highest collective angles where the error exceeds 6%. The larger errors which occur in the torque coefficients are possibly due to the two-dimensional drag table used in the code. (It should be remarked here that in this comparison there has been none of the traditional varying of collective angle to obtain a good C_T, C_Q match.) The generally good thrust prediction seems to indicate that the assumption of fully developed vortex strength is correct. However, this assumption will now be further checked by a direct analysis of the hot-wire wake measurements.

TABLE 1.- THRUST AND TORQUE COEFFICIENTS

	MEASUREMENTS				PREDICTIONS			
AR = 13.7 R = 105.20 cm c = 7.62 cm	$\theta_{c(ROOT)}$	θ_{c75}	C_T	$C_Q \times 10^{-3}$	C_T	$C_Q \times 10^{-3}$	Γ_{MAX}	FM
UN-TWISTED BLADE	5°	5°	0.0018	0.109	0.0018	0.108	0.0120	0.48
	8°	8°	0.0037	0.253	0.0037	0.219	0.0193	0.73
	12°	12°	0.0056	0.493	0.0059	0.436	0.0292	0.73
AR = 13.7 R = 105.20 cm c 7.62 cm TWISTED BLADE	11.4°	5.3°	0.0018	0.111	0.0020	0.108	0.0080	0.57
	14.8°	8.7°	0.0038	0.279	0.0038	0.223	0.0170	0.75
	18.4°	12.3°	0.0054	0.458	0.0059	0.409	0.0260	0.78
	13.0°	6.9°	0.0026	0.134	0.0027	0.163	0.0123	0.66
	15.9°	9.8°	0.0042	0.344	0.0043	0.271	0.0194	0.74
	19.6°	13.5°	0.0059	0.569	0.0063	0.488	0.0286	0.73
AR = 6 R = 114.3 cm c = 19.05 cm UN-TWISTED BLADE	8°	8°	0.0046	——	0.0048	0.452	0.252	0.52
	12°	12°	0.0079	——	0.0083	0.958	0.415	0.56

As in Refs. [1] and [4], the vortex strength can be computed after making the following assumptions:

1) The hot wire measures no flow components parallel to the vortex axis.

2) The vortex is assumed to be locally indistinguishable from a two-dimensional line vortex; i.e., the curvature of the helical vortex is ignored and the measured vortex is assumed to be axisymmetric about its axis.

3) The vortex is assumed to evolve sufficiently slowly that the timewise stream of data can be used to infer the spacial vortex structure.

4) The residual velocity of vortices is assumed to be constant. For young vortices (under 90° old, for a two-bladed rotor), this constant is usually assumed to be the vortex translation velocity.

In Ref. [1], the strength of the vortex was found by fitting the induced velocity expression for a two-dimensional vortex to the measured data. This expression is

$$\frac{V_i}{\Omega R} = A(d) \frac{\Gamma_{max}/\Omega R^2}{2\pi(d/R)}$$

where the strength of the vortex is given by A(d), the ratio of the vortex circulation to the maximum bound circulation of the blade. The method of Ref. [1] was to vectorially add V_I and the residual velocity V_R, and then choose a constant value of $A(d) = A_V$ which gave a best fit to the measured velocity-magnitude history. Such a fit is shown in Fig. 4(a).

In the present work, a different approach is taken to finding the vortex strength, since the goal is now to determine the entire circulation variation A(d). In this case, the vortex trajectory data are used to express the measured vortex velocity magnitude data as a spacial function. The assumed residual velocity plus the known location of the vortex with respect to the probe permits the

determination of V_i, and hence the circulation A(d), as a simple quadratic function of the measured velocity magnitude. Figure 4(b) shows a typical variation of A as a function of distance, d, from the center of the vortex. This figure shows the circulation asymptotically approaching the maximum bound circulation for the untwisted low aspect ratio data described in Ref. [1].

In the region far away from the center of the vortex, small changes in the velocity (due to errors in residual velocity, calibration, signal noise, etc.) cause large changes in circulation, making this region particularly susceptible to error. In particular, the assumption that V_R is constant and equal to the translation velocity is frequently unreliable. This is demonstrated in a comparison of Figs. 4 and 5, which differ only in having different assumed V_R's. In Fig. 5, V_R is chosen to equal the translation velocity V_{TR}, and it is seen that the circulation in the far inviscid field decreased unrealistically rather than remaining constant. In Fig. 4, V_R is chosen to be $0.25V_{TR}$, and this circulation remains properly constant. Notice in Fig. 5, however, that the maximum indicated circulation is very close to that in Fig. 4. We have always found that, even with an incorrect value of V_R, this maximum indicated circulation is quite accurate. An additional source of error is that the vortex circulation is normalized by a computed rather than a measured value of Γ_{max}. (It was shown in Ref. [1] that the accuracy of the A.M.I. code, HOVER, was about 5%.) With all these possible error sources, the maximum value of A(d) (that is, the vortex strength) was always between 0.9 and 1.1 (for the twisted and untwisted blades, as well as the low aspect ratio blades of Ref. [1]). Figures 6 to 9 show some typical results for untwisted blades at 8° and 12° collective pitch, and twisted blades at 9.8° and 13.5°.

It therefore appears that, contrary to Ref. [4], there is little reason to doubt the complete vortex roll-up assumption for typical planforms, twist distributions, or operating conditions. The next step in the analysis is to investigate the effect of twist, aspect ratio, and operating condition on the inner vortex structure.

4. Vortex Structure

The fixed-wing trailing vortex has been a subject of considerable study [5, 6,7,8,9]. As a general rule, these vortices are turbulent and can be divided into four distinct flow regions (see Fig. 10):

(I) Viscous Core. This innermost region is dominated by viscous diffusion rather like the laminar sublayer of a turbulent boundary layer. Rotation is solid-body type and circulation varies as the square of distance from the center.

(II) Turbulent Mixing Region. In this region, flow is dominated by turbulent diffusion. It is in this region, at the maximum velocity radius r_1, that the tangential velocity attains its maximum value. The circulation here is a logarithmic function of radius [5,7].

(III) Transition Region. Here, the turbulent region makes the transition to the outer inviscid region. This is an extremely variable region, and it is difficult to generalize the circulation distribution here. This transition is not smooth for young vortices and seems to occur in discrete jumps. These jumps are due to the vorticity sheet spiraling into the vortex.

(IV) Irrotational Region. In this outermost region, circulation is constant.

The above classification agrees well with the observed rotor vortices. This is seen in Fig. 1 , which is a re-plot of the untwisted blade data of Fig. 7. In this figure, the distance, d, is normalized by the maximum velocity radius, r_1, and plotted logarithmically in order to better see the small inner core. The viscous Region I is seen as a smooth region extending to about $d/r_1 = 0.9$. Beyond this point and extending to about $d/r_1 = 3.0$ is an obviously turbulent region whose variation on this semilogarithmic plot can be reasonably fitted to a straight line — this is Region II. Beyond this point is a region which shows considerable variation between different vortex traces. In the midst of this variability, there is one feature which frequently appears. This is a more or less discontinuous jump in the circulation. In Fig. 11, the circulation seems to be asymptotically approaching a constant value of $A = 0.8$ until $d/r_1 = 9.0$, at which point A jumps to a new value of 0.95. At $d/r_1 = 22$, an additional jump to $A = 1.0$ occurs and indicates the beginning of Region IV. The noise which is seen in this outermost region in this figure is due to the previously mentioned sensitivity of the method. In fact, an inspection of the original velocity data (Fig. 7) shows that at this point the velocity variation suddenly becomes quite smooth. This sudden change in signal character is frequently, but not always, seen at the beginning of Region IV.

In order to see the effect of the blade loading on the vortex structure, it is necessary to compare different blade load variations that have the same maximum circulation value. The twisted blade which corresponds to the above untwisted blade at 12° collective has a $\theta_{c_{75}}$ of 13.5°. A circulation plot for this case is shown in Fig. 12 (this is a semilogarithmic replot of Fig. 9). This figure compares quite closely with that for the untwisted blade (Fig. 11 vs. Fig. 12). For this twisted blade case, the boundary between Regions I and II occurs at about 0.75 (rather than 0.9 for the untwisted case), and the boundary between Regions II and III occurs at 2.0 (rather than 3.0). Again, there are two circulation jumps in Region III occurring at 5.0 and 16.0 (rather than 9.0 and 22.0). As in the previous case, the final jump marks the beginning of Region IV and a sudden decrease in the measured velocity roughness. Similar comparisons (with some minor variations) of the twisted and untwisted blade wakes have been obtained for other collective angles. Figure 13 shows the untwisted blade wake for a collective of 8°, and Fig. 14 shows the corresponding twisted blade data. The latter twisted blade data closely fit the previously described vortex structure. However, the corresponding untwisted blade data differ somewhat in that only one circulation jump is seen in Region III. The low aspect ratio data of Ref. [3] have also been analyzed using the above method. Figure 15 shows the vortex structure from an untwisted blade, AR = 6, $\theta_c = 8°$. The general structure of this vortex closely corresponds to the high aspect ratio data, except that the signal is so noisy that circulation jumps cannot be readily discerned. Figure 16 shows low aspect ratio vortex data for a collective of 12°. This case is unique in that the inner core region is much larger ($r_1 = 0.008R$) than in all the previously mentioned cases. Besides this difference, however, the vortex is essentially identical to all the previous cases. All the previous data are for young vortices (less than 90° old). Figure 17 is typical of data from older vortices and displays a structure very similar to young vortex data, except that circulation jumps are no longer present.

In all the above data, there is frequently a greater variation between two successive vortices than there is between those for differing blades and collective angles. The resulting uncertainty band for the data is shown in Fig. 18. A curve (also shown in Fig. 18) which best fits the data can be written as:

Region I	$A = 0.37\ (d/r_1)^2$	$0 \le d/r_1 \le 0.73$
Region II	$A = 0.32 + 0.39\ \ell n(d/r_1)$	$0.73 \le d/r_1 \le 3.0$
Region III	$A = 1 - 1.2\ e^{-0.52(d/r_1)}$	$3.0 \le d/r_1$

where an average value of r_1 is 0.003R. The only data which do not fit the above curve are those for the low aspect ratio, 12° collective case. The only reason for this difference is that the core radius r_1 is quite different, for this case $r_1 \cong 0.008R$.

Although the proportionality constant (0.39) in the logarithmic term shows little variation from the average for the conditions tested, these results do not necessarily suggest a possible universality of the constant as in the case of the turbulent boundary-layer theory. From the fixed-wing measurements, Corsiglia et al. [9] reported an average value of 0.44 for this proportionality constant. Hoffmann and Joubert [5] and Phillips [6] obtained a value of about 0.5. McCormick et al. [10], based on the results from a full-scale airplane, got a value of 0.16. This constant may vary with tip geometry and have a weak dependence on the Reynolds number. More tests are required to verify such suggestions.

5. Concluding Remarks

The present study is aimed at an understanding (or at least a description) of the effects of blade twist and aspect ratio on the geometry and flow structure of rotary-wing tip vortices. The main tools for this study are a combined use of hot-wire probe, six-component balance, and a hover performance code (A.M.I.'s code, HOVER) to determine blade-load distribution. This load distribution was related to the vortex flow structure which is obtained from the hot-wire output.

The main conclusions from this study are:

1. Vortex trajectories obtained from high aspect ratio blades compare quite closely with previous published data. However, at the lower aspect ratio the vortex geometry does not agree well with other published data. In all cases, the present measured vortex geometries are consistent with measured or computed loading.

2. For the present high aspect ratio blades, there is no measurable effect of blade twist on vortex strength or flow structure. In all cases, complete vortex roll-up occurs.

3. The vortex flow is generally turbulent. This structure may be conveniently divided into four distinct regions, namely: a laminar inner region, a turbulent logarithmic region, a transition region, and an irrotational outer region. Almost all the vortex structure data fit a single empirically obtained curve.

ACKNOWLEDGEMENTS

The authors would like to extend their thanks to Georgene Laub and Robert George, who tirelessly and ably assisted in the running of the experiment. Special thanks should also go to Jim McCroskey and Fred Schmitz for their helpful suggestions.

REFERENCES

1. F. X. Caradonna, C. Tung — Experimental and Analytical Studies of a Model Helicopter Rotor in Hover. Presented at the 6th European Rotorcraft and Powered Lift Aircraft Forum, Bristol, England, Sept. 1980.

2. J. D. Kocurek, J. L. Tangler — A Prescribed Wake Lifting Surface Hover Performance Analysis. Presented at the 32nd Annual National Forum of the American Helicopter Society, May 1978, Preprint 1001.

3. J. M. Summa, D. R. Clark — A Lifting-Surface Method for Hover/Climb Loads. Presented at the 35th Annual Forum of the American Helicopter Society, Washington, D.C., May 1979, Preprint 79-1.

4. C. V. Cook — The Structure of Rotor Blade Tip Vortex. AGARD CP-111, Sept. 1972.

5. E. R. Hoffman, P. N. Joubert — Turbulent Line Vortices. J. of Fluid Mechanics (1963) 16, Part 3.

6. W. R. C. Phillips — The Turbulent Trailing Vortex During Roll-Up. J. of Fluid Mechanics (1981) 105.

7. P. G. Saffman — Structure of Turbulent Line Vortices. The Physics of Fluids (1973) 16 (8).

8. J. N. Nielsen, R. G. Schwind — Decay of a Vortex Pair Behind an Aircraft; Aircraft Wake Turbulence and its Detection. Edited by J. Olson, A. Goldberg, and M. Roger, Plenum Press, New York (1971).

9. V. R. Corsiglia, R. G. Schwind, N. A. Chigier — Rapid Scanning, Three-Dimensional Hot-Wire Anemometer Surveys of Wing-Tip Vortices. J. of Aircraft (1973) 10 (12).

10. B. W. McCormick, J. L. Tangler, H. E. Sherrieb — Structure of Trailing Vortices. J. of Aircraft (1968) 5 (3).

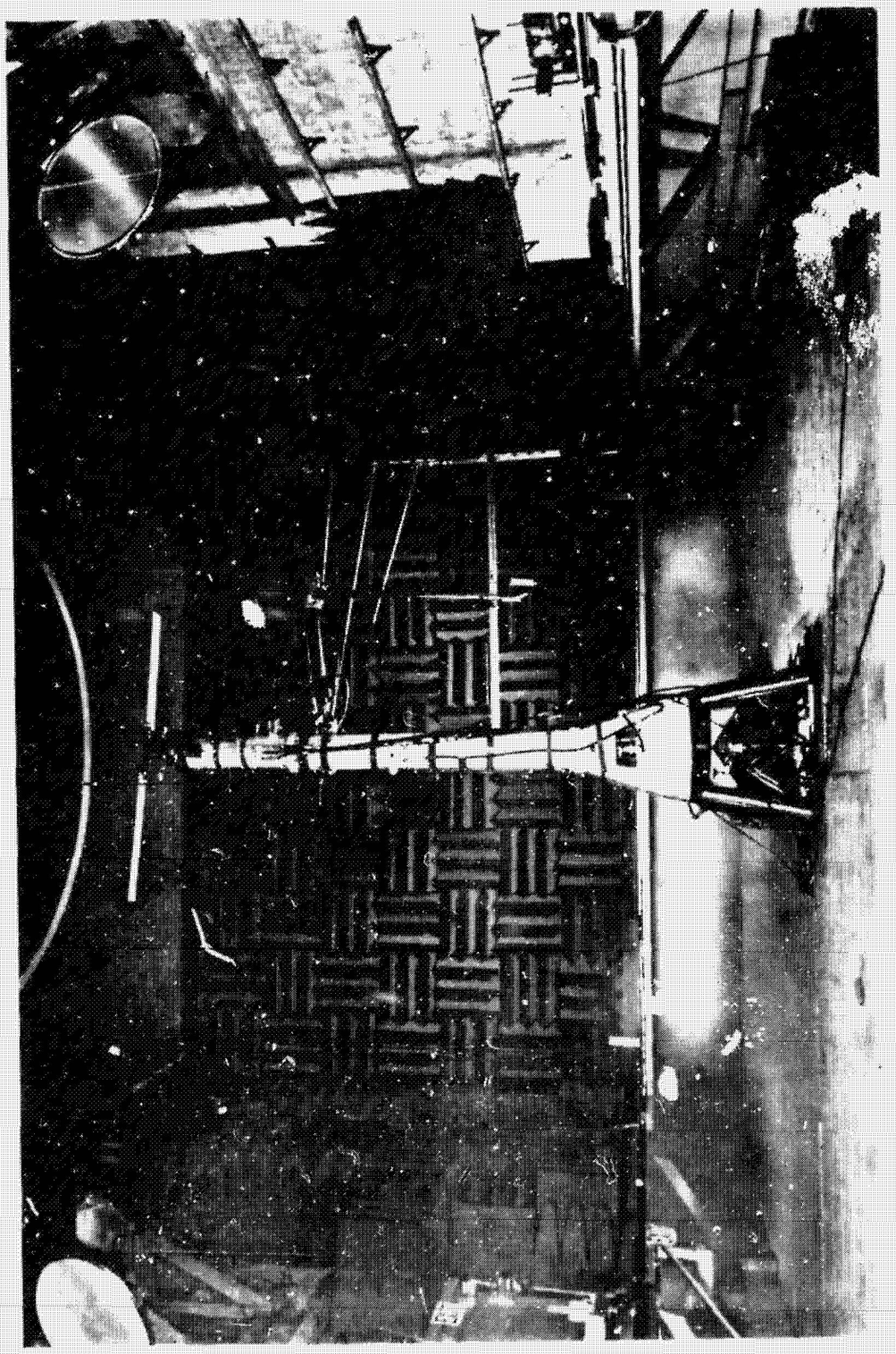

Fig. 1. The model and experimental set-up.

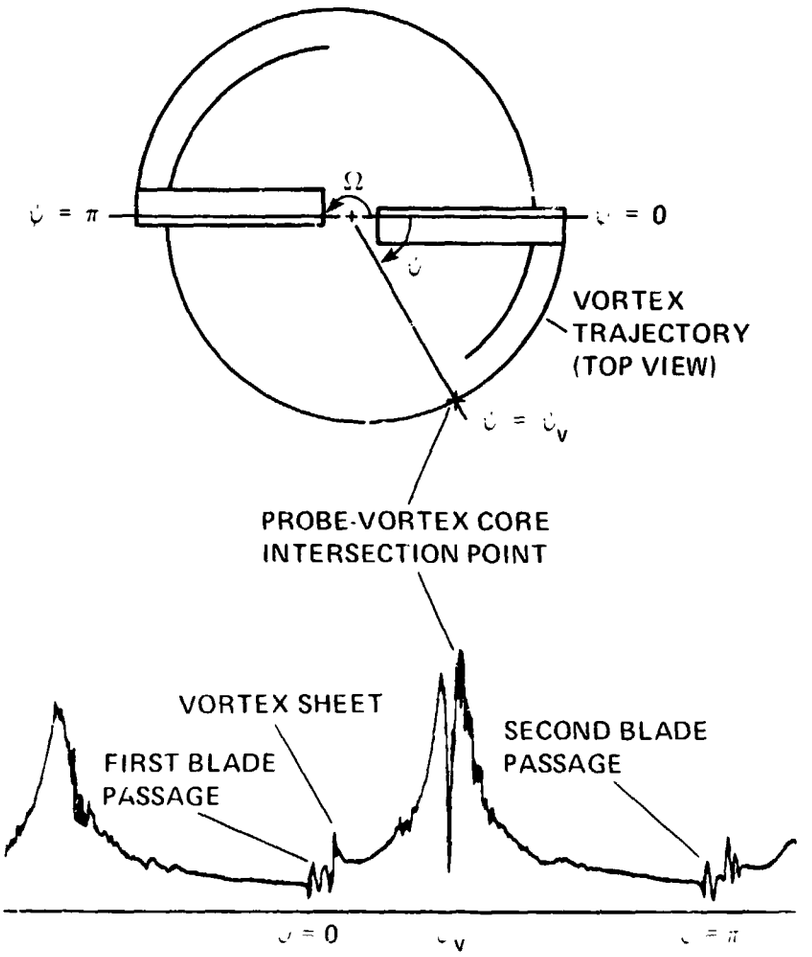

Fig. 2. Typical wake probe data.

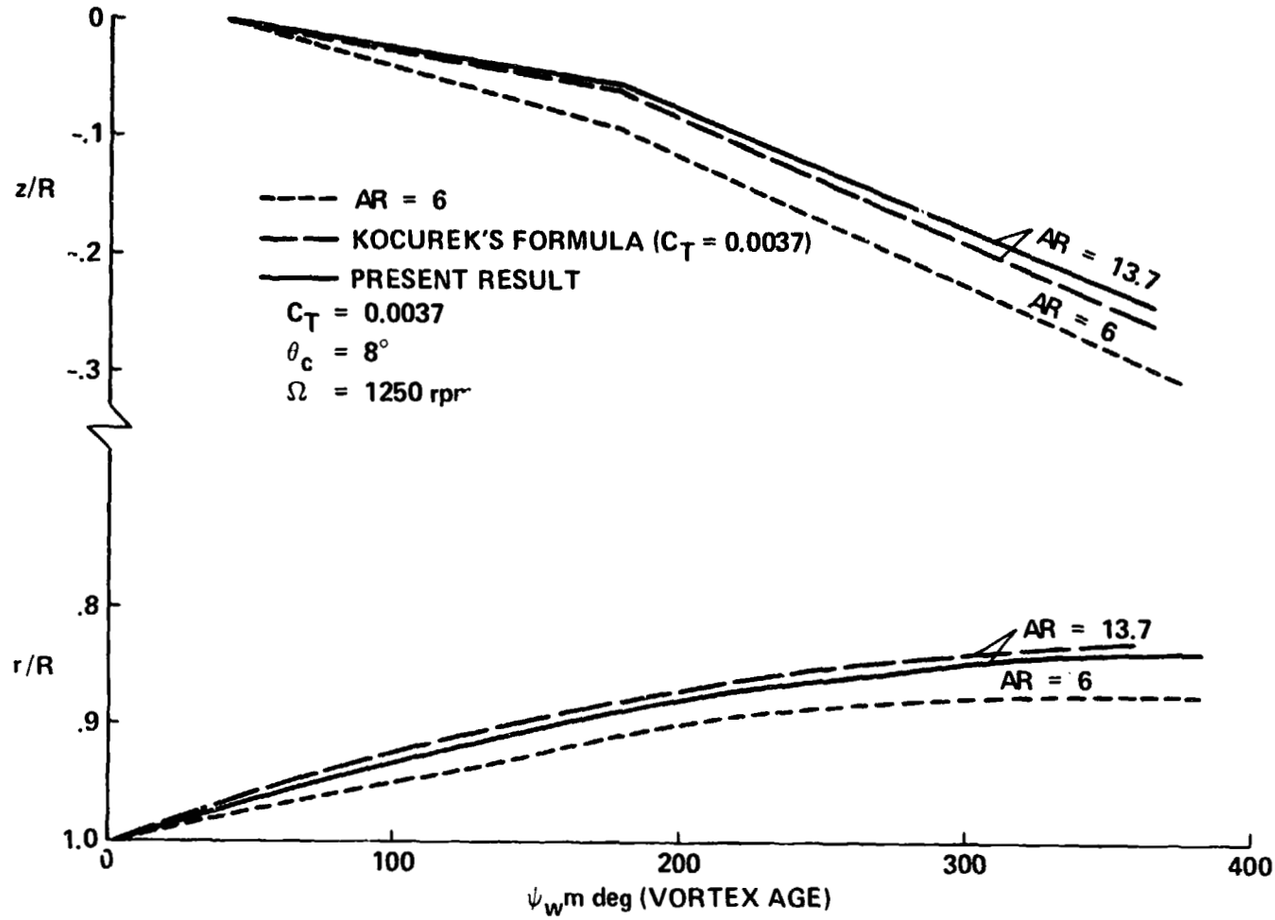

Fig. 3. Wake geometry measurement for $\theta_c = 8°$ and comparison with classical data and low aspect ratio rotor blade.

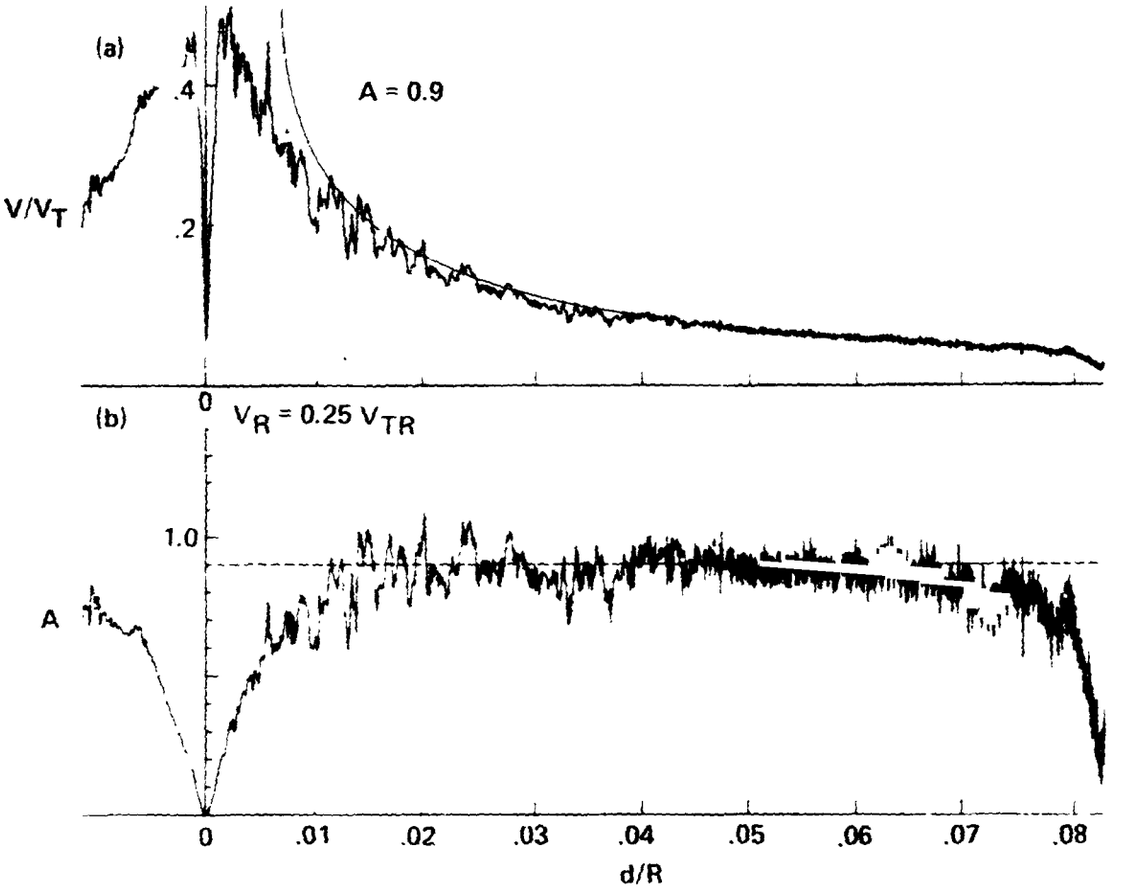

Fig. 4. Circulation and tangential velocity profiles and A/d curve fit. AR = 6.0; collective pitch, θ_c = 8°; vortex age, ψ = 53.8°; $V_R = 0.25V_{TR}$.

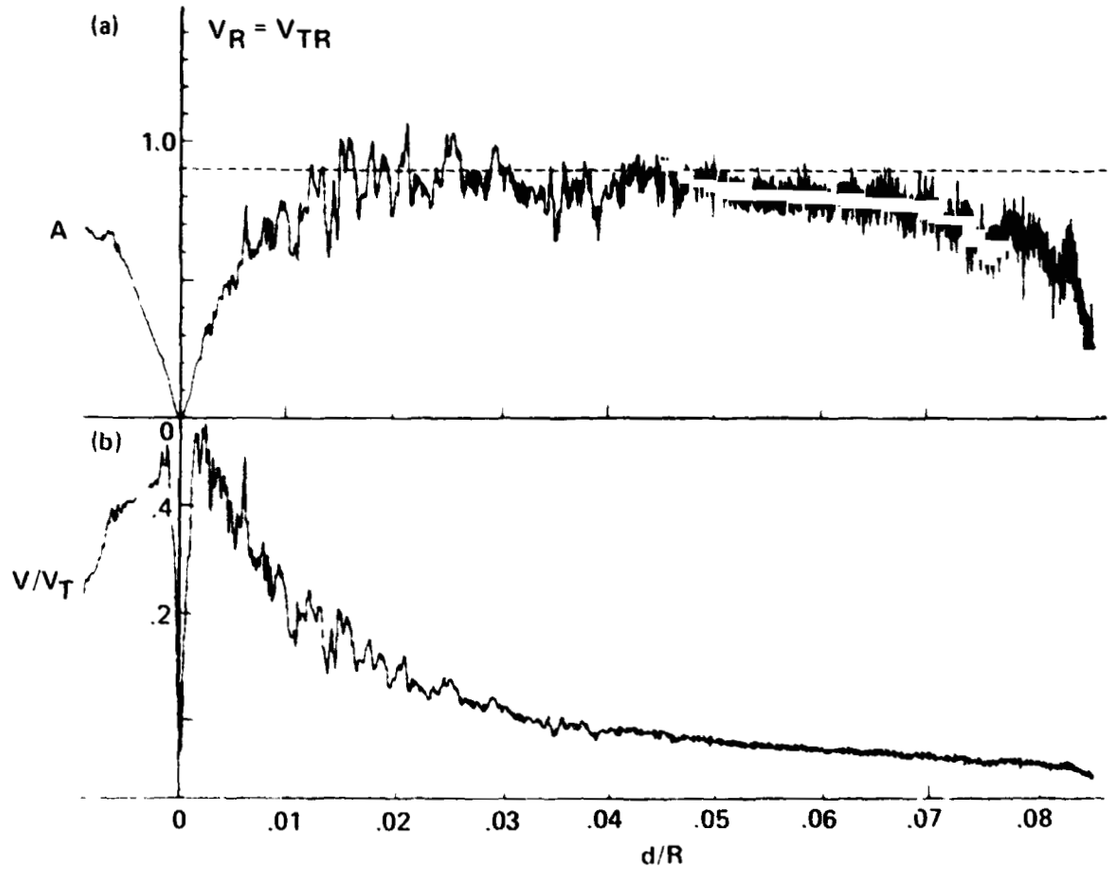

Fig. 5. Effect of residual velocity on circulation profile. AR = 6.0; collective pitch, θ_c = 8°; vortex age, ψ = 53.8°; $V_R = V_{TR}$.

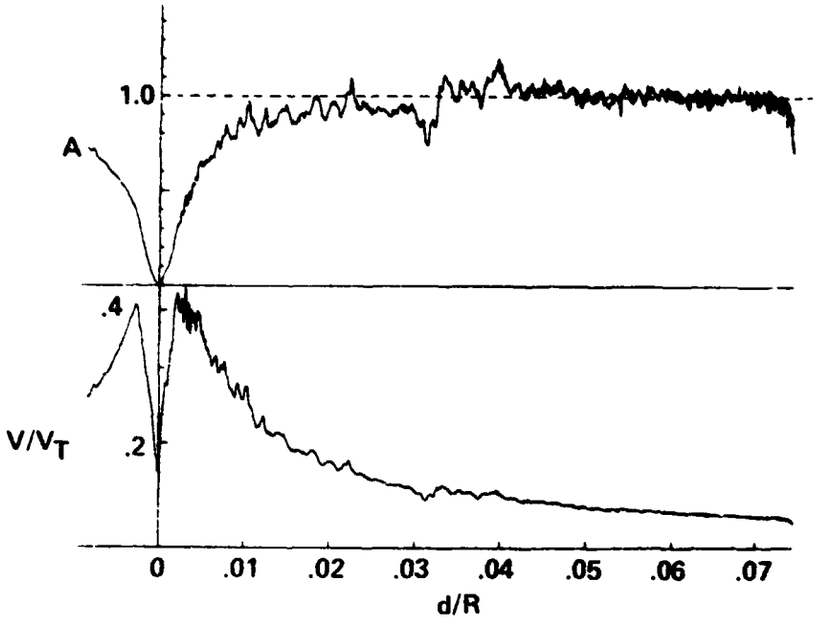

COLLECTIVE PITCH, θ_c = 8°; VORTEX AGE, ψ = 57.5°

Fig. 6. Circulation and tangential velocity profiles for untwisted blade.

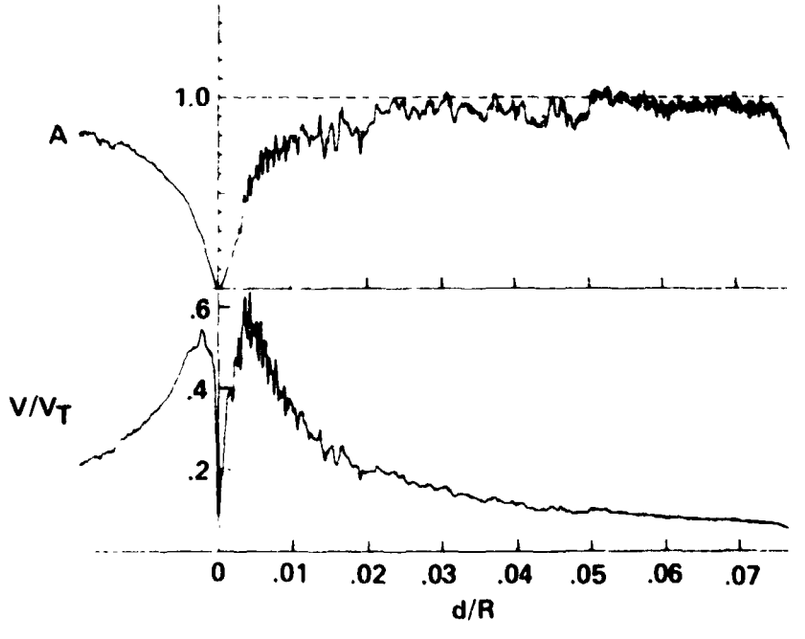

COLLECTIVE PITCH, θ_c = 12°; VORTEX AGE, ψ = 76.3

Fig. 7. Circulation and tangential velocity profiles for untwisted blade.

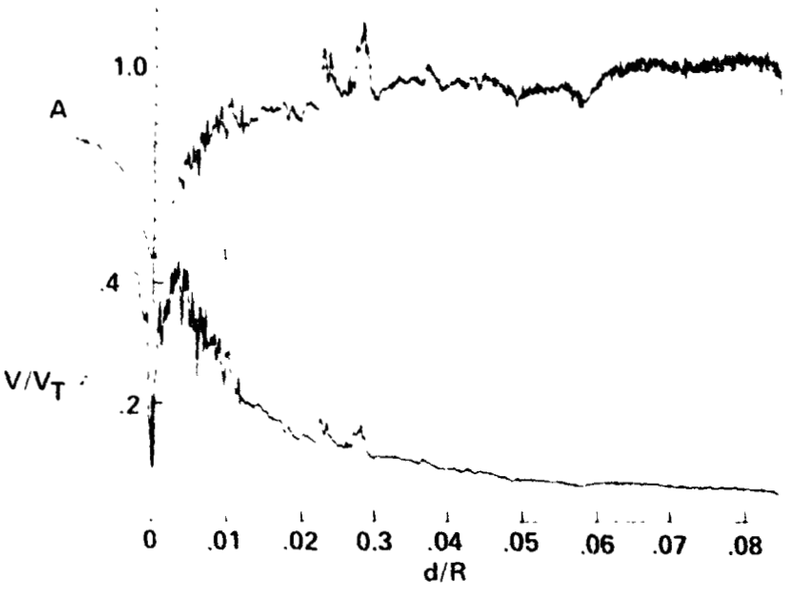

COLLECTIVE PITCH, θ_c = 9.8°; VORTEX AGE, ζ = 65.4

Fig. 8. Circulation and tangential velocity profiles for twisted blade.

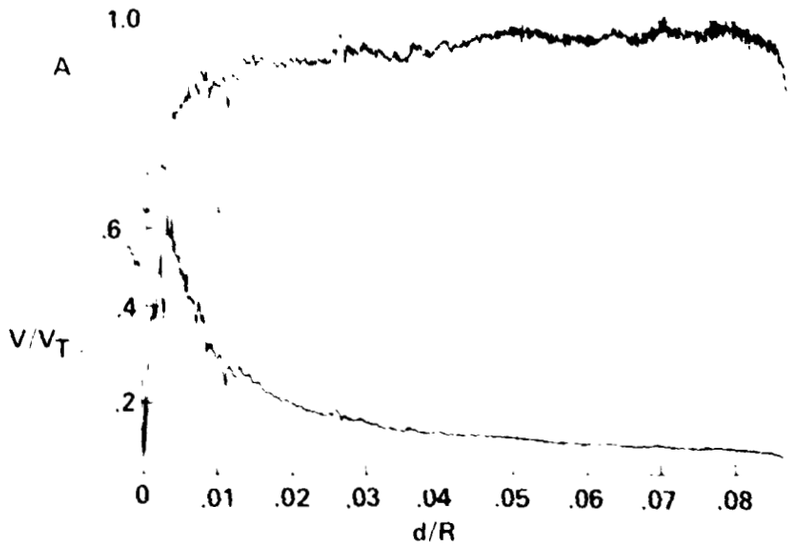

COLLECTIVE PITCH, θ_c = 13.5°; VORTEX AGE, ζ = 58.4°

Fig. 9. Circulation and tangential velocity profiles for twisted blade.

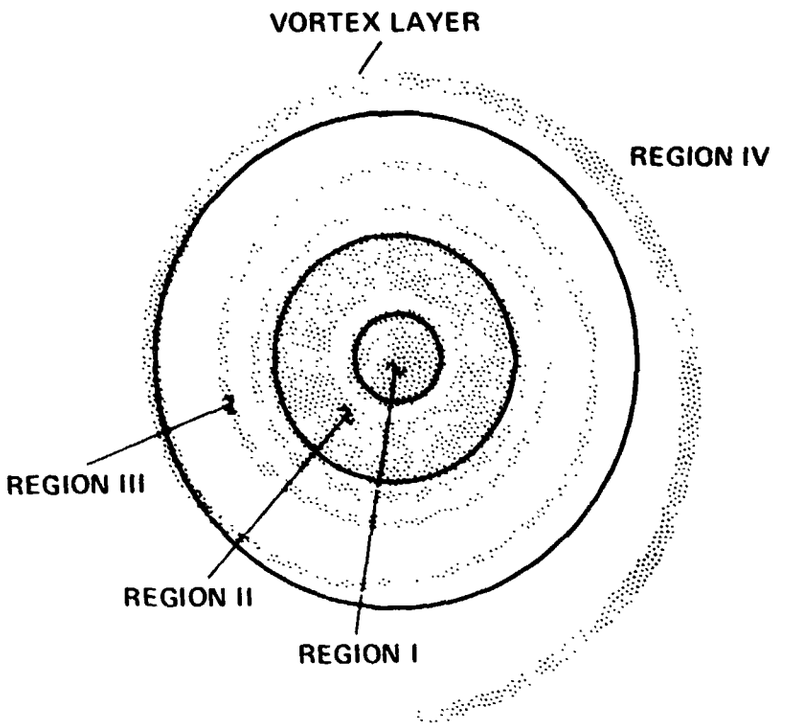

Fig. 10. Sketch of roll-up and merging of a trailing vortex layer.

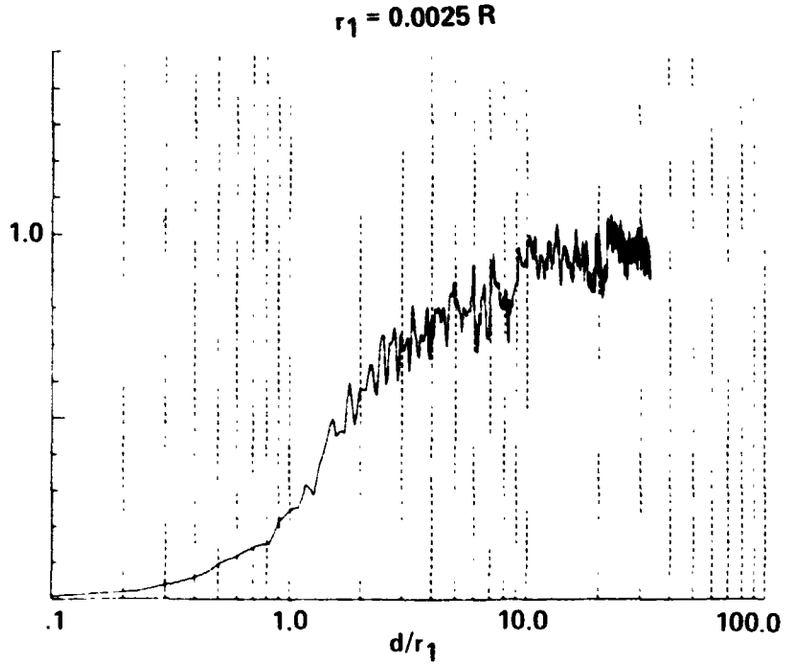

COLLECTIVE PITCH, θ_c = 12° ; VORTEX AGE = 76.3°

Fig. 11. Circulation profile for untwisted blade.

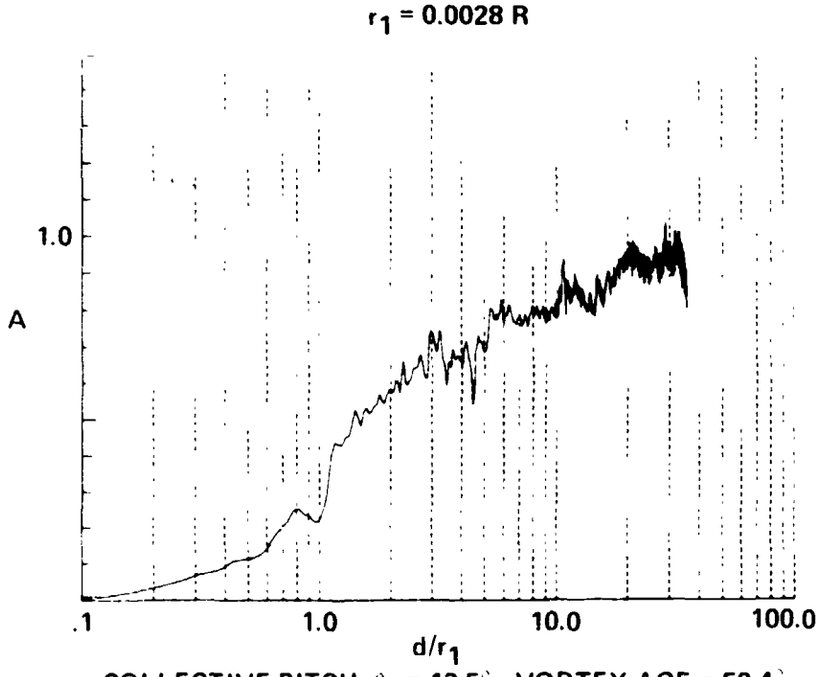

COLLECTIVE PITCH, θ_c = 13.5° ; VORTEX AGE = 58.4°

Fig. 12 Circulation profile for twisted blade.

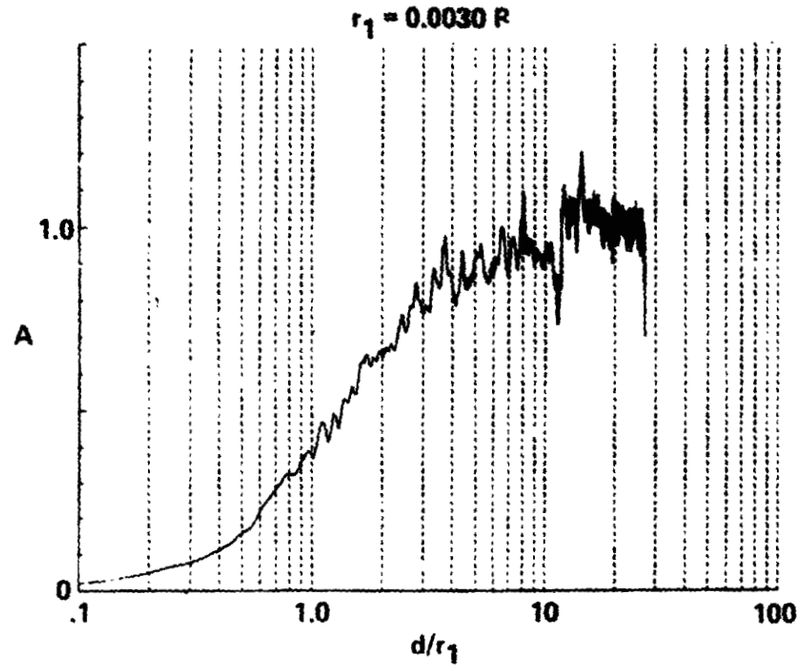

COLLECTIVE PITCH, θ_c = 8°; VORTEX AGE, ψ = 57.5°

Fig. 13. Circulation profiles for untwisted blade.

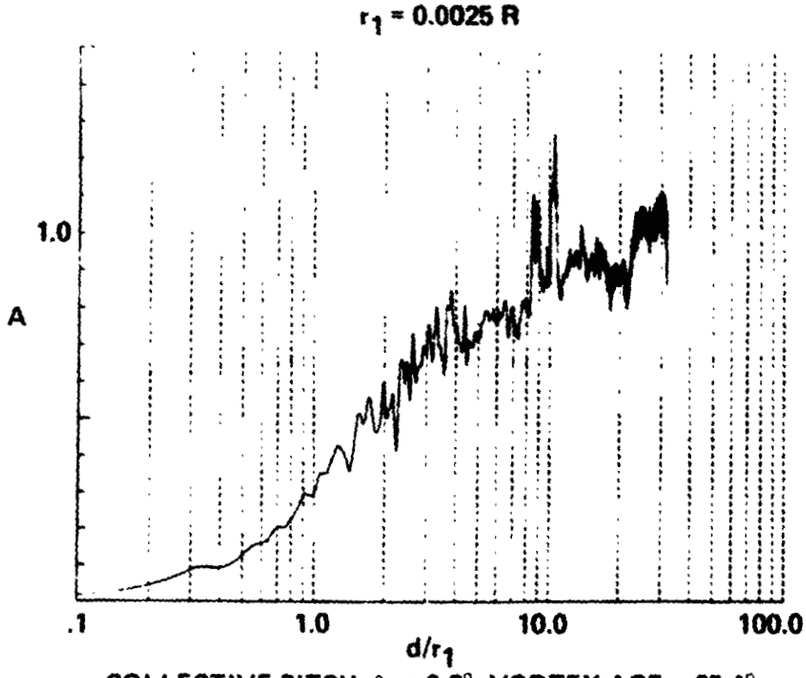

COLLECTIVE PITCH, θ_c = 9.8°; VORTEX AGE = 65.4°

Fig. 14. Circulation profiles for twisted blade.

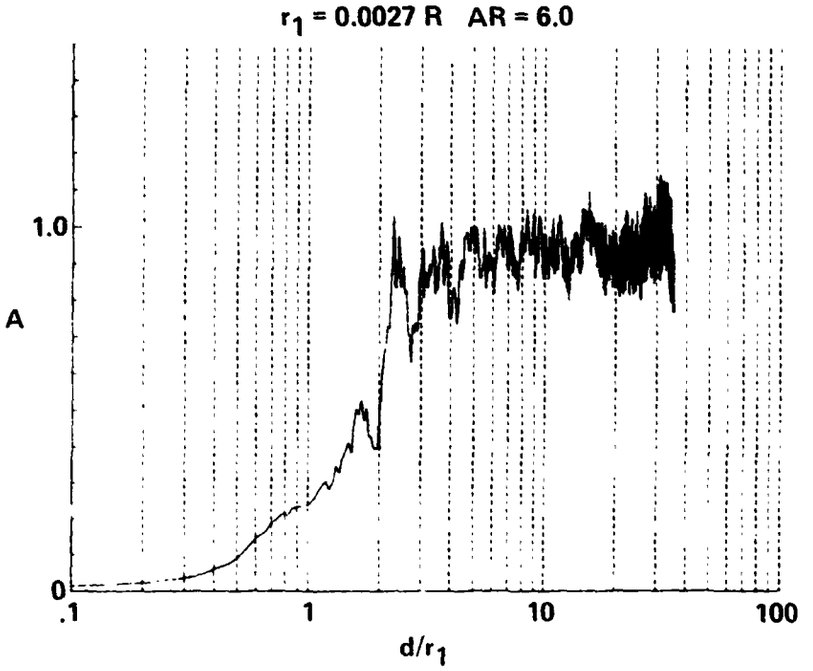

COLLECTIVE PITCH, θ_c = 8°; VORTEX AGE, ψ = 50.5°

Fig. 15. Circulation profile for untwisted blade.

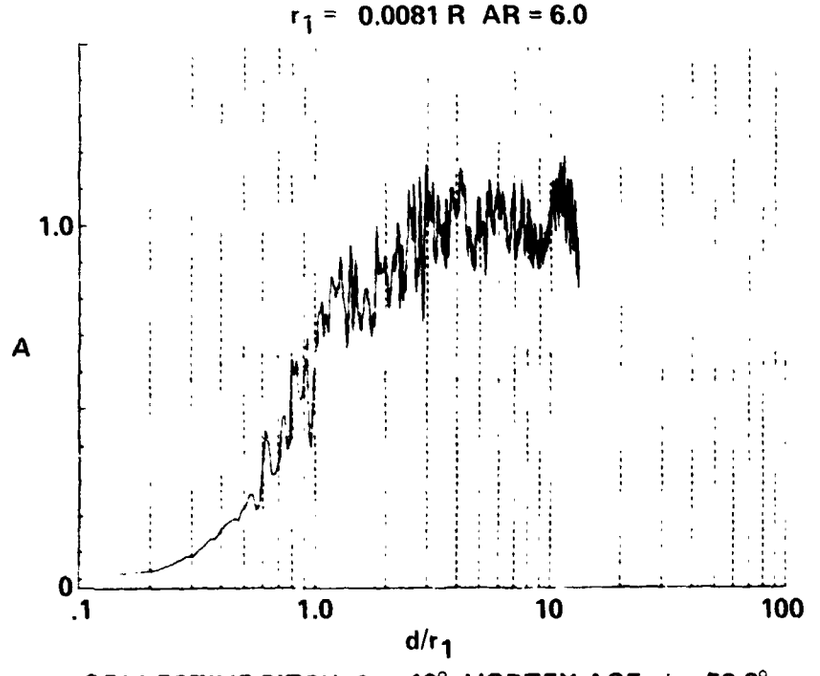

COLLECTIVE PITCH, θ_c = 12°; VORTEX AGE, ψ = 52.2°

Fig. 16. Circulation profile for untwisted blade.

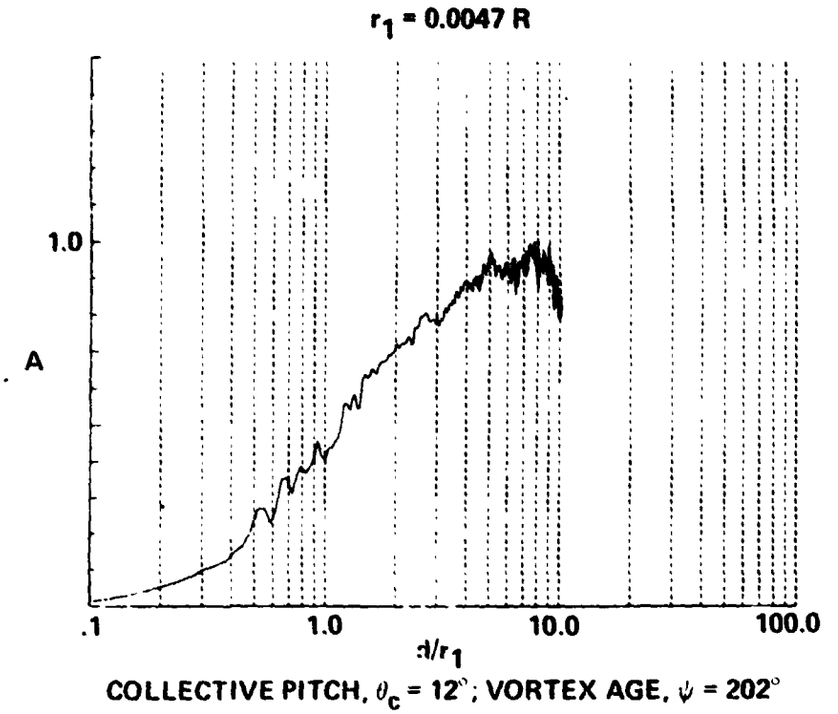

Fig. 17. Circulation profile for twisted blade.

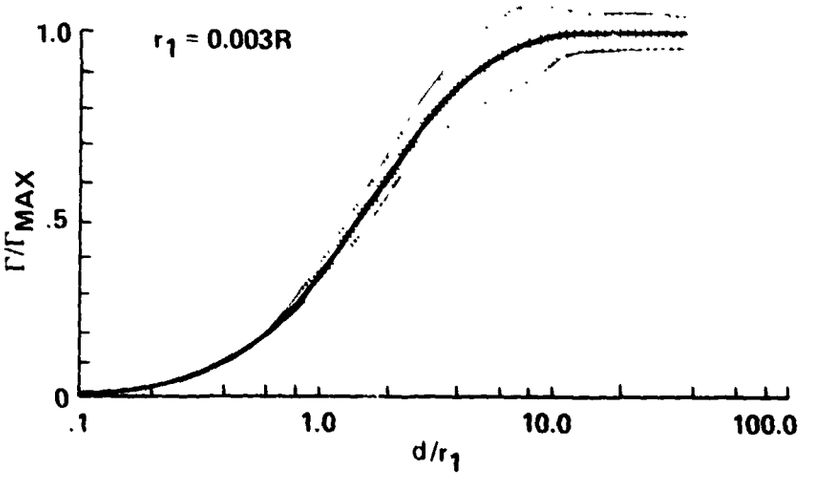

Fig. 18. Empirical circulation profile.